

Article

Path-Tracking Ability of the ASV on Different Adhesion Coefficient Roads Based on Slide Mode Control

Shengzhi Zhong^{1,2}, Dengzhi Peng³ , Bin Huang^{1,*} and Liutao Ma¹

¹ Hubei Key Laboratory of Advanced Technology for Automotive Components, Wuhan University of Technology, Wuhan 430070, China; zhongshengshi@wuling.com.cn (S.Z.)

² Liuzhou Wuling New Energy Automobile Co., Ltd., Wuhan 430070, China

³ Dongfeng Off-Road Vehicle Co., Ltd., Shiyan 442013, China; pengdengzhi@whut.edu.cn

* Correspondence: huangb@whut.edu.cn

Abstract: A vehicle equipped with an articulated steering system is often used in a particular area, such as a mine or the construction field. These sealing or semi-sealing fields make autonomous driving by an ASV (Articulated Steering Vehicle) easier than in passenger cars. Path-tracking is essential for an autonomous vehicle. To improve the path-tracking ability of an ASV, a path-tracking model is established based on dynamic theory. Then, the slide-mode predictive-control (SMPC) strategy is initiated to design the path-tracking controller. The improvement in the path-tracking ability on roads with different adhesion coefficients is validated via the HIL (Hardware in Loop) platform. According to the simulation in HIL with the provided strategy, the path-tracking error during the typical condition decreased by 21.73~93.84%, demonstrating the SMC controller can be used to improve the path-tracking performance of an ASV.

Keywords: path-tracking; ASV; SMPC



Citation: Zhong, S.; Peng, D.; Huang, B.; Ma, L. Path-Tracking Ability of the ASV on Different Adhesion Coefficient Roads Based on Slide Mode Control. *Electronics* **2024**, *13*, 105. <https://doi.org/10.3390/electronics13010105>

Academic Editor: Felipe Jiménez

Received: 5 December 2023

Revised: 24 December 2023

Accepted: 25 December 2023

Published: 26 December 2023



Copyright: © 2023 by the authors. Licensee MDPI, Basel, Switzerland. This article is an open access article distributed under the terms and conditions of the Creative Commons Attribution (CC BY) license (<https://creativecommons.org/licenses/by/4.0/>).

1. Introduction

Normally, a vehicle equipped with an articulated steering system is identified as an ASV (Articulated Steering Vehicle). The unique mechanical structure of the articulated steering system allows the vehicle to have a lower steering radius. Thus, it is quite common in engineering, such as mining vehicles and loaders. Developing autonomous or remote-controlled ASVs will ease the burden on the drivers. Environmental perception, path planning, and path-tracking are the three vital operations for an autonomous vehicle. Compared to a normal passenger car, these ASVs often operate in closed areas. These areas have lower interference but worse road conditions than paved roads [1]. There are still some challenges for autonomous passenger cars [2]. Because of the simpler working conditions and fewer challenges for autonomous ASVs, it may be easier to apply the technology in these situations. Thus, it is necessary and meaningful to improve the path-tracking ability of the ASV.

For the passenger car, plenty of work has been done to enhance the path-tracking ability [3]. A simultaneous path following the control method was presented based on a 4WD-4WIS (Four-wheel Drive and Four-wheel Independent Steering) autonomous vehicles in [4]. In the work by Zhang, L., the AFS (Active Front Steering System) and differential braking system were coordinated to improve the path-tracking ability of an autonomous vehicle [5]. J Yu J. combined the robust MPC (Model Predictive Control) and optimal preview controller to maintain the path-tracking error of a passenger car [6]. The algorithm was validated by simulation with different road friction coefficients, bank angles, and vehicle mass uncertainty. A path-tracking control algorithm was designed for an AGV (Autonomous Ground Vehicle) based on the linear parameter-varying system. It controls the vehicle path at different velocities and road friction coefficients [7]. In these works, the strategy was similar. Usually, it comprises three units: the reference model; upper layer

controller; and lower layer for the sub-control system, such as DYC (Direct Yaw Control), AFS, or ABA (Active Brake Assist).

The dynamic model for vehicles with articulated steering systems and regular cars has been developed, and the analysis and optimization process of path-tracking ability can be taken as a reference.

Due to the structural characteristic of an ASV, its reference model is different from a vehicle with an Ackerman steering system. For the ASV, studies have developed dual-parts, equivalent skid and slip, and recombined methods to build the reference model. In the dual-parts method, an articulated joint connects the front and rear of the vehicle. The rear component is taken as an extra mass attached to the front component, according to the articulated joint [8]. For the equivalent skip and slip model, the ASV is simplified as two skids, two slips, and a hinge that connects them into a whole system [9]. During the steering process, the vehicle's center of mass changes as the angle varies between the front and rear components.

The path-tracking control strategy can be categorized as a model-free algorithm, a model-based algorithm, and a learning-based control [10].

The common model-free algorithms include PID, SMC (Sliding Mode Control), and fuzzy logic control. The PID control method is frequently used in engineering due to its simple structure and straightforward design and implementation [11]. However, its disadvantages are also well-known. Regulating the nonlinear system and system uncertainty is difficult. Furthermore, the low adaptive ability of the control parameters in diverse working conditions is of concern. Some hybrid algorithms have been developed based on PID to deal with the situation [12]. The fuzzy control has been used to adjust the control parameter to avoid the manual parameter adjustment process [13]. Peng, D. established an anti-windup PID controller based on the Gaussian function to adjust the parameters in the PID controller [14]. The SMC is known as a nonlinear feedback control. It has the advantage of being immune to external disturbances and its fast reaction [15]. However, chattering may occur when the input changes to a high frequency. Thus, the second-order SMC was designed based on the first-order SMC with an improved power-added integrator technique [16]. The fuzzy-SMC was provided to adjust the sliding mode boundary thickness and gain coefficient. With the structural asymmetry of the fuzzy rule, the trajectory tracking error is minimized [17]. The fuzzy logic control contains four major steps: fuzzification; fuzzy rules; fuzzy interference; and defuzzification. The fuzzy rule is the key to achieving good fuzzy logic control. The determination of the fuzzy rule relies on expert experience, which often needs a large amount of experimental data. The optimization algorithm was combined with fuzzy control to improve its performance. The fuzzy controller was optimized by a genetic method to maintain path-tracking accuracy while improving vehicle stability [18]. The PSO (Particle Swarm Optimization) has been used in the fuzzy controller to achieve a better path-tracking effect and self-adaptability [19].

Compared to the model-free algorithm, the model-based algorithm needs more mathematical model details. The typical model-based algorithm is LQR (Linear Quadratic Regulator) and MPC. The LQR can achieve a balance between the control effort and the system by adjusting the weight value or matrix represented by Q and R [20]. It has strong robustness for linear control systems [21]. Normally, the value of Q and R is determined based on experience [22]. To acquire better control results, the value of Q and R can be gained by optimization methods, such as PSO and a GA (Genetic Algorithm) [23]. The MPC can achieve feedback correction and prediction for a system with multiple constraints and feedback. It maintains the accuracy of path tracking and vehicle stability by considering the vehicle's dynamic constraints [24]. However, its high complexity requires a higher performance process [25]. Bai, G. took a mining vehicle with an articulated steering system as an example and provided a nonlinear model predictive controller to lower the path tracking error when the operating speed of the vehicle increased from 2 m/s to 4 m/s [26]. Huang, B. designed an AMPC (Adaptive Model Predictive Controller) to lower the path tracking error for an ASV [27].

A typical learning-based method is reinforcement learning. Its performance can be enhanced gradually with a large amount of training data. An innovative self-learning system based on reinforcement learning has been provided for an unmanned surface vehicle. It only uses the input and output signals [28]. Ma Haitong developed a model-based feasibility enhancement technique of constrained reinforcement learning that can enhance the feasibility of policies using a generalized control barrier function that is defined based on the distance to the constraint boundary [29].

For ASVs, it usually works in a worse condition than the passenger car. Therefore, maintaining its stability while tracking the reference path is quite important. According to the current work, two major components are important to achieve this goal: the path-tracking model and the control strategy. In this case, the path-tracking model is based on the recombination structure model, which has better accuracy than the normal model. An integrated adaptive feedback control (AFC) and SMC are provided to maintain the tracking ability on the road with high and low adhesion coefficients.

2. Model Establishment and Validation

2.1. Path-Tracking Model

A vehicle is a complicated dynamic system with lots of DOFs (Degrees of freedom). The simplified model with 2 DOFs is taken as the reference model to maintain efficiency. The dual-parts and equivalent slip and slip models ignore the mass variation during the steering process. To improve the accuracy, the recombination structure model considers the mass variation. In the recombination structure model, the front and rear components recombined as a new vehicle with the shifted mass center during the steering process. The diagram of this model is illustrated in Figure 1. In Figure 1, the actual mass center is identified as O_a .

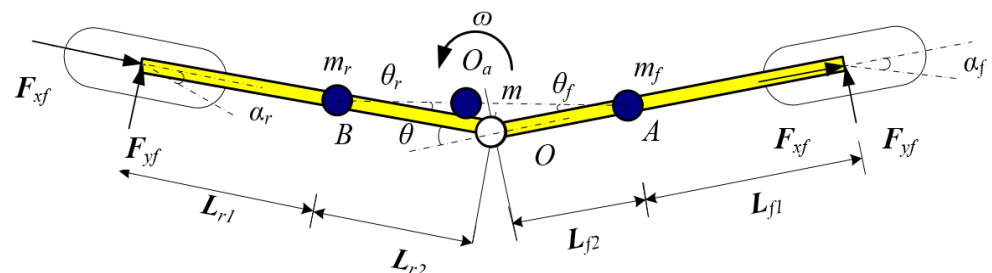


Figure 1. Recombination structure model.

According to the geometry relationship demonstrated in Figure 1, the distance between the front and rear components of the recombined vehicle can be gained by Equation (1), according to the cosine law.

$$L_{fr} = \sqrt{L_{f2}^2 + L_{r2}^2 + 2L_{f2}L_{r2} \cos \theta} \tag{1}$$

$$\begin{cases} L_{Oaf} = \frac{m_r L_{fr}}{m_f + m_r} \\ L_{Oar} = \frac{m_f L_{fr}}{m_f + m_r} \end{cases} \tag{2}$$

$$\begin{cases} \frac{\sin \theta_f}{\sin \theta} = \frac{L_{r2}}{L_{fr}} \\ \frac{\sin \theta_r}{\sin \theta} = \frac{L_{f2}}{L_{fr}} \end{cases} \tag{3}$$

where

$$\begin{aligned} I_w \dot{\omega} &= (L_{f1} + L_{Oaf} \cos \theta_f) F_{yf} - (L_{r1} + L_{Oar} \cos \theta_r) F_{yr} \\ &\approx (L_{f1} + L_{Oaf}) F_{yf} - (L_{r1} + L_{Oar}) F_{yr} \end{aligned} \tag{4}$$

$$\begin{cases} \dot{Y} = v_x \sin \varphi + v_y \cos \varphi \\ \dot{\varphi} = \omega \\ m(\dot{v}_y + v_x \omega) = F_{yf} + F_{yr} \\ I_z \dot{\omega} = (L_{f1} + L_{Oaf})F_{yf} - (L_{r1} + L_{Oar})F_{yr} \end{cases} \quad (5)$$

in which Y is the lateral displacement of the vehicle, v_x and v_y are the longitudinal and lateral speeds of the vehicle; φ denotes the vehicle yaw angle, ω represents the yaw rate; m is the vehicle mass; F_{yf} and F_{yr} represent the lateral force of the front and rear axles; I_z is the yaw moment of inertia.

Based on the geometry analysis in Figure 1, the tire sideslip angle in this model can be gained by Equation (6).

$$\begin{cases} \alpha_f = \beta + \frac{(L_{f1} + L_{Oaf})\omega}{v_x} - \theta_f \\ \alpha_r = \beta - \frac{(L_{r1} + L_{Oar})\omega}{v_x} - \theta_r \end{cases} \quad (6)$$

The lateral force of the tires on the front and rear axles can be obtained by the following equation:

$$\begin{cases} F_{yf} = k_f \alpha_f \\ F_{yr} = k_r \alpha_r \end{cases} \quad (7)$$

in which k_f and k_r mean the equivalent cornering stiffness of tires on the front and rear axles. The path-tracking model of an articulated vehicle can be transferred into Equation (8).

$$\begin{cases} \dot{Y} = v_x \sin \varphi + v_y \cos \varphi \\ \dot{\varphi} = \omega \\ \dot{v}_y = \frac{1}{m} \left[k_f \left(\beta + \frac{(L_{f1} + L_{Oaf})\omega}{v_x} - \theta_f \right) + k_r \left(\beta - \frac{(L_{r1} + L_{Oar})\omega}{v_x} - \theta_r \right) \right] - v_x \omega \\ \dot{\omega} = \frac{1}{I_z} \begin{bmatrix} (L_{f1} + L_{Oaf})k_f \left(\beta + \frac{(L_{f1} + L_{Oaf})\omega}{v_x} - \theta_f \right) \\ -(L_{r1} + L_{Oar})k_r \left(\beta - \frac{(L_{r1} + L_{Oar})\omega}{v_x} - \theta_r \right) \end{bmatrix} \end{cases} \quad (8)$$

2.2. Model Validation

The established path-tracking model needs to be validated before further application because it is different from the classical vehicle dynamic model for regular passenger cars. The vehicle trajectory and yaw rate were recorded by the GPS (Global Position System) and IMU (Inertial Measurement Unit) mounted on the ASV (As shown in Figure 2). The articulated angle was calculated based on the distance between the front and rear components. The distance value was acquired from a distance sensor. The details of the sensors in the test are listed in Table 1.

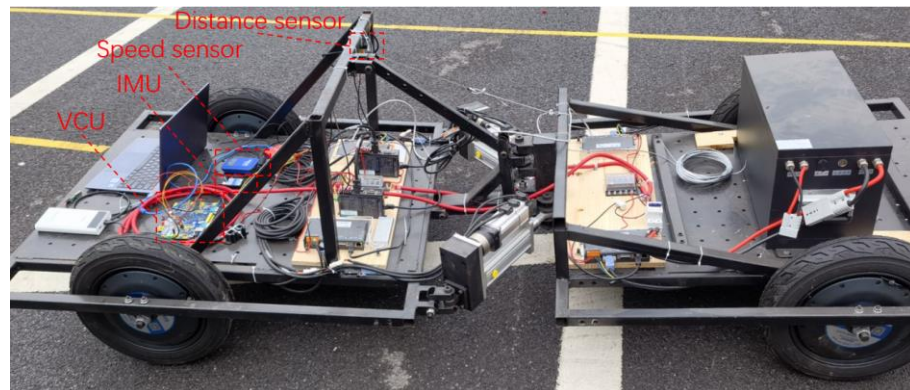


Figure 2. Field test scenario.

Table 1. Sensors in the field test.

No	Sensor	Measured Parameter	Type	Sampling Frequency (Hz)
1	Distance sensor	Distance	BRT38-0.5M-COM1024-DC24	20
2	Speed sensor	Speed, Location	V-box	20
3	IMU	Yaw rate	SST 810	100

The step input of the articulated angle was taken as the field test scenario. The acquired vehicle yaw rate and location data were compared to the corresponding value gained from the established model, as shown in Figures 3 and 4.

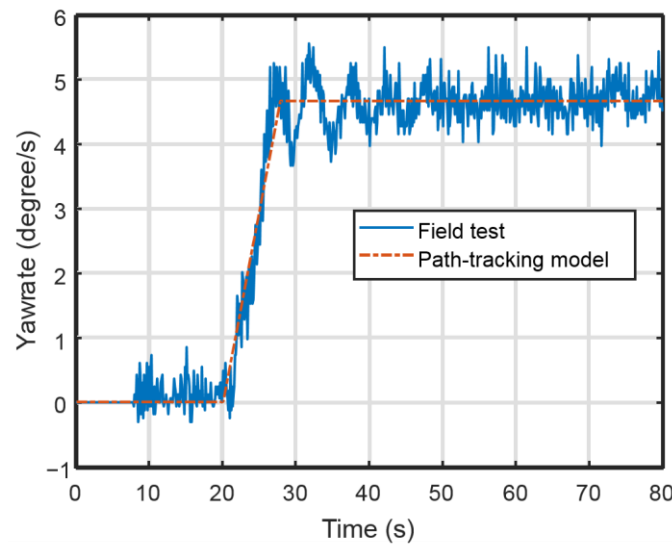


Figure 3. Comparison of vehicle yaw rate.

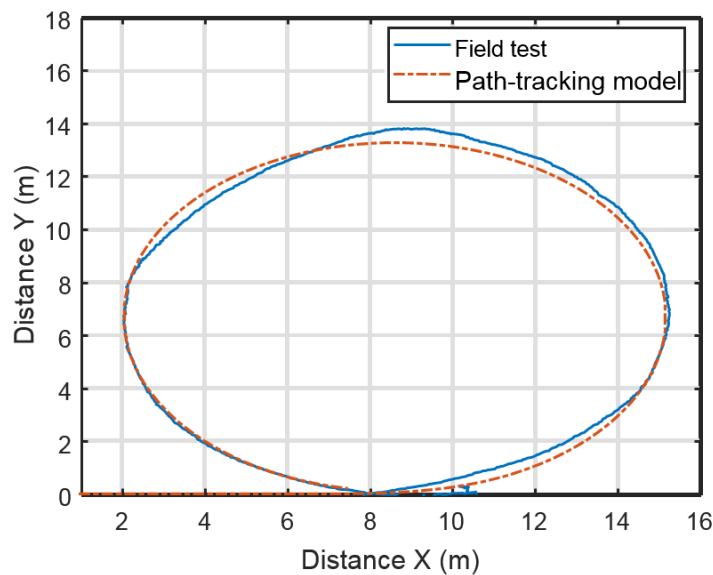


Figure 4. Comparison of vehicle trajectory.

The illustrations in Figures 3 and 4 show that the calculated vehicle yaw rate and trajectory are in good correlation with the test data. Thus, the built path-tracking model could accurately demonstrate an ASV’s dynamic characteristics.

3. Controller Design

3.1. Slide-Mode Prediction Controller

The concept of SMPC is building the basic predictive model with a sliding mode function using MPC’s prediction and feedback correction method to obtain a controller with the advantage of these two algorithms. The SMPC can avoid the influence of uncertain factors and oscillations on the sliding surface [30]. The process of the SMPC is similar to MPC in that it comprises three major steps: prediction; updating; and feedback correction (shown in Figure 5). The prediction is achieved based on the sliding mode value and historical information. The updating process refers to repeatedly optimizing the input to enable the index function of the system to become closer to the global optimization. Feedback correction is to diminish the influence of prediction deviation.

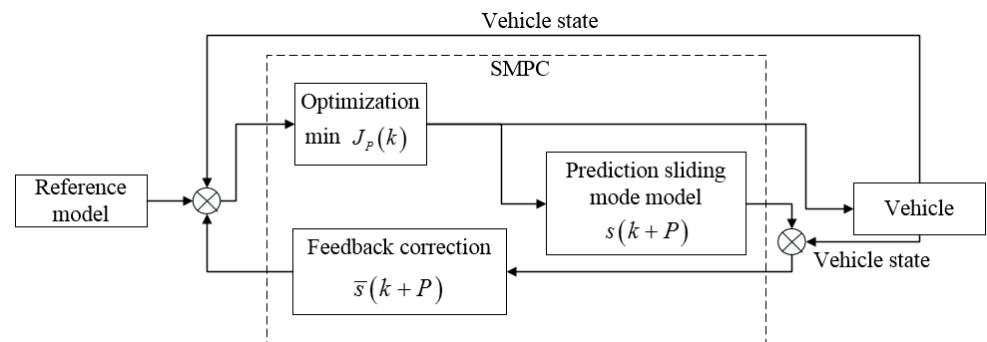


Figure 5. The process of an SMPC.

A linear discrete-time system’s state–space function can be described as follows.

$$\begin{cases} x(k + 1) = Ax(k) + Bu(k) \\ y(k) = Cx(k) \end{cases} \quad (9)$$

in which $x(k)$ represents the state vector of the system, $u(k)$ is the control vector, $y(k)$ means the system output vector. The system matrix, input, and output matrix are represented by A , B , and C , respectively. The output error of the system can be gained based on the system output vector and the expected value of the system output.

$$e(k) = y(k) - y_d(k) \quad (10)$$

The sliding mode function of the system can be defined as follows:

$$s(k + 1) = \sigma e(k + 1) \quad (11)$$

in which $\sigma = [\sigma_1, \dots, \sigma_n]^T$, where its value can be determined by the classical pole configuration or quadratic optimization method. Therefore, the system’s dynamic characteristics and stability can be optimized. The sliding surface of the system can be obtained by $S = \{e(k) | s(e(k)) = 0\}$.

Based on Equations (9)–(11), the future sliding mode output at the time $k + P$ can be obtained, as shown in Equations (12) and (13).

$$s(k + P) = \sigma e(k + P) \quad (12)$$

$$s(k + P) = \sigma C \begin{bmatrix} A^P x(k) + \sum_{i=1}^{P-1} A^{P-i} Bu(k + i - 1) \\ + \sum_{i=1}^{P-N} A^{i-1} Bu(k + N - 1) \end{bmatrix} - \sigma y_d(k + P) \quad (13)$$

in which P means the prediction time domain, and N means the control time domain. Using a similar method, we can obtain historical information at the time $k - P$.

$$s(k - P) = \sigma C \left[\begin{array}{l} A^P x(k - P) + \sum_{i=1}^{N-1} A^{P-i} B u(k - P + i - 1) \\ + \sum_{i=1}^{P-N} A^{i-1} B u(k - P + N - 1) \end{array} \right] - \sigma y_d(k) \quad (14)$$

Equation (13) can be sorted as follows.

$$S(k + 1) = Gx(k) + \Theta U(k) - \sigma Y_d(k) \quad (15)$$

in which $S(k + 1)$, $U(k)$, $Y_d(k)$, G and Θ are defined in Equations (16)–(20).

$$S(k + 1) = [s(k + 1) \quad s(k + 2) \quad \cdots \quad s(k + P)]^T \quad (16)$$

$$U(k) = [u(k) \quad u(k + 1) \quad \cdots \quad u(k + N - 1)]^T \quad (17)$$

$$Y_d(k) = [y_d(k + 1) \quad y_d(k + 2) \quad \cdots \quad y_d(k + P)]^T \quad (18)$$

$$G = [\sigma CA \quad \sigma CA^2 \quad \cdots \quad \sigma CA^P]^T \quad (19)$$

$$\Theta = \begin{bmatrix} \sigma CA & 0 & \cdots & \cdots & 0 \\ \sigma CAB & \sigma CB & 0 & \cdots & 0 \\ \cdots & \cdots & \ddots & \cdots & 0 \\ \sigma CA^{N-1}B & \sigma CA^{N-2}B & \cdots & \sigma CAB & \sigma CB \\ \sigma CA^N B & \sigma CA^{N-1}B & \cdots & \sigma CA^2 B & \sigma CAB + \sigma CB \\ \vdots & \vdots & \cdots & \vdots & \vdots \\ \sigma CA^{P-1}B & \sigma CA^{P-2}B & \cdots & \sigma CA^{P-N+1}B & \sum_{i=0}^{P-N} \sigma CA^i B \end{bmatrix} \quad (20)$$

Normally, there are certain deviations in the mathematical model of sliding-mode prediction due to the system’s time lag, nonlinearity, and external disturbance. Hence, the current actual measured value corrected the future sliding-mode predicted value $s(k)$, and the history value $s(k|k - P)$, and the future prediction value were gained by the mathematical model $s(k|k + P)$. The corrected future sliding-mode predicted value $\bar{s}(k + P)$ can be expressed as:

$$\bar{s}(k + P) = s(k + P) + h_p[s(k) - s(k|k - P)] \quad (21)$$

in which h_p is the feedback correction coefficient. Rewriting Equation (21) in the vector form produces Equation (22).

$$\bar{S}(k + 1) = S(k + 1) + HE(k) \quad (22)$$

$$\bar{S}(k + 1) = [\bar{s}(k + 1) \quad \bar{s}(k + 2) \quad \cdots \quad \bar{s}(k + P)]^T \quad (23)$$

$$E(k) = S(k) - S_P(k) \quad (24)$$

$$S(k) = [s(k) \quad s(k) \quad \cdots \quad s(k)]_{1 \times P}^T \quad (25)$$

$$S_P(k) = [s(k|k - 1) \quad s(k|k - 2) \quad \cdots \quad s(k|k - P)]^T \quad (26)$$

$$H = \text{diag}[h_1 \quad h_2 \quad h_3 \quad h_4] \quad (27)$$

To solve the optimal control output of the system based on the MPC theory, the sliding-mode error and system input are taken as the system optimization indicators, and the cost function can be determined by Equation (28).

$$J_P(k) = \sum_{i=1}^P q_i [\bar{s}(k+i) - s_r(k+i)]^2 + \sum_{j=1}^N r_j [u(k+j-1)]^2 \tag{28}$$

in which q_i and represents the weight coefficient of the two indicators, and $s_r(k+i)$ means the reference value of the sliding mode.

The exponential approach law was chosen as the sliding-mode reference value to acquire the desired control performance, as shown in Equation (29).

$$\begin{cases} s_r(k+P) = (1 - qT)s_r(k+P-1) - \epsilon T \tanh(s_r(k+P)) \\ s_r(k) = s(k) \end{cases} \tag{29}$$

Rewriting the cost function in Equation (28) in the vector form, as shown in Equation (30), the corresponding weight coefficient matrix is shown in Equations (31) and (32).

$$J_P(k) = \|\bar{S}(k+1) - S_r(k+1)\|_Q + \|U(k)\|_R \tag{30}$$

$$= [Gx(k) + \Theta U(k) - \sigma Y_d(k)]$$

$$Q = \text{diag}[q_1 \quad q_2 \quad \cdots \quad q_P] \tag{31}$$

$$R = \text{diag}[r_1 \quad r_2 \quad \cdots \quad r_N] \tag{32}$$

3.2. Path-Tracking Controller

The vehicle’s lateral distance, yaw angle, lateral velocity, and yaw rate were chosen as the state vector in the path-tracking process x .

$$x = [Y \quad \varphi \quad v_y \quad \omega_r]^T \tag{33}$$

For the output vector $y = [Y \quad \varphi]^T$, the articulated angle was set as the control input, thus, $u = \theta$. The system matrix A , input matrix B , and output matrix C are defined in Equations (34)–(36).

$$A = \begin{bmatrix} 1 & \Delta T(v_x \cos \varphi - v_y \sin \varphi) & \Delta T \cos \varphi & 0 \\ 0 & 1 & 0 & \Delta T \\ 0 & a_{32} & 1 + \Delta T \frac{k_r - k_f}{mv_x} & -\Delta T v_x \\ 0 & 0 & a_{43} & a_{44} \end{bmatrix} \tag{34}$$

$$\begin{cases} a_{32} = \Delta T \left(\frac{k_f(L_{f1} + L_{Oaf}) - k_r(L_{r1} + L_{Oar})}{mv_x} - v_x \right) \\ a_{43} = \Delta T \frac{k_f(L_{f1} + L_{Oaf}) - k_r(L_{r1} + L_{Oar})}{I_z v_x} \\ a_{44} = 1 + \Delta T \frac{k_f(L_{f1} + L_{Oaf})^2 - k_r(L_{r1} + L_{Oar})^2}{I_z v_x} \end{cases} \tag{35}$$

$$B = \begin{bmatrix} 0 & 0 & \Delta T \frac{k_f L_{r2} + k_r L_{f2}}{m L_{fr}} & \Delta T \frac{k_f L_{r2}(L_{f1} + L_{Oaf}) - k_r L_{f2}(L_{r1} + L_{Oar})}{I_z L_{fr}} \end{bmatrix} \tag{36}$$

$$C = [1 \quad 1 \quad 0 \quad 0] \tag{37}$$

The constraint should consider the input and vehicle dynamic limitation during the path-tracking process. Thus, the constraints during the process can be summarized as follows:

$$\begin{cases} \theta_{\min} \leq u \leq \theta_{\max} \\ \alpha_{f\min} - \zeta \leq \alpha_f \leq \alpha_{f\max} + \zeta \\ \alpha_{r\min} - \zeta \leq \alpha_r \leq \alpha_{r\max} + \zeta \end{cases} \tag{38}$$

in which θ_{\min} and θ_{\max} mean the minimum and maximum articulated angle of the vehicle, $\alpha_{f\min}$, $\alpha_{f\max}$, $\alpha_{r\min}$, and $\alpha_{r\max}$ represent the minimum and maximum sideslip angle of the front and rear tires, ζ is the slack factor. The output range of the system can be adjusted dynamically by setting the value of ζ .

4. Path-Tracking Performance Validation

To validate the effectiveness of the designed path-tracking controller, a double-lane change was implemented in the hardware in the loop (HIL) platform. As shown in Figure 6, in the HIL, the designed strategy was set in the dSPACE MicroAutoBox, and the vehicle dynamic model, motor control model, and road model were simulated in the SCALEXiO unit. The dSPACE MicroAutoBox acted as the VCU for ASV, while the ASV and road were simulated in the SCALEXiO unit. The data in these units were sent to the platform for data visualization.

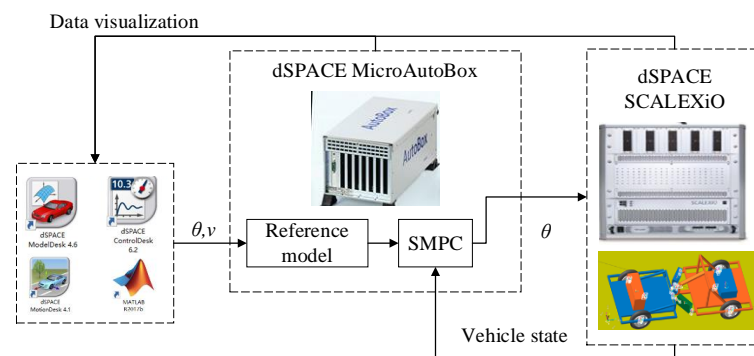


Figure 6. HIL platform.

A double-lane change is one of the most common work conditions used to validate vehicle path-tracking performance. During the test, the vehicle shifts to another routine from the original path and returns to the original path without hitting the boundary (red lines) in Figures 7 and 8. A double-lane change initiated on a road with high and low road cohesion coefficients was simulated in this case. Considering the low stability of an ASV, the vehicle speed was set to 60 km/h. The vehicle trajectory and yaw rate during the double-lane change process are illustrated in Figures 7 and 8.

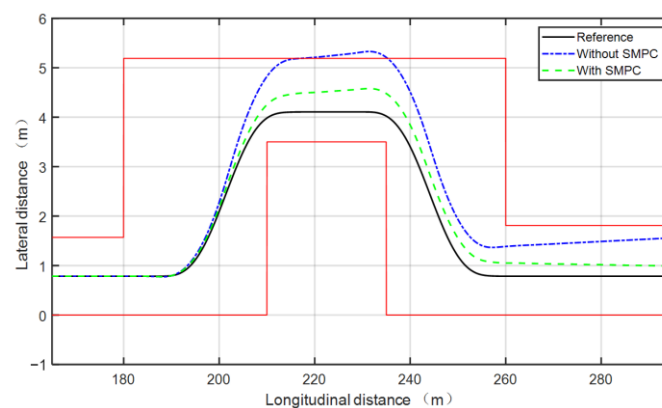


Figure 7. Comparison of vehicle trajectory ($\mu = 0.8$).

As shown in Figure 7, without an SMPC, the gap between the ASV’s lateral distance and reference became larger over the course of the double-lane change. At the end of the process, the trend of the lateral distance continued to increase. For the ASV with an SMPC, the overall error of lateral distance was smaller, and the lateral distance converged.

As shown in Figure 8, with an SMPC, the dwell time of the vehicle’s yaw rate between the ASV and reference model was smaller, and it had a smaller peak value.

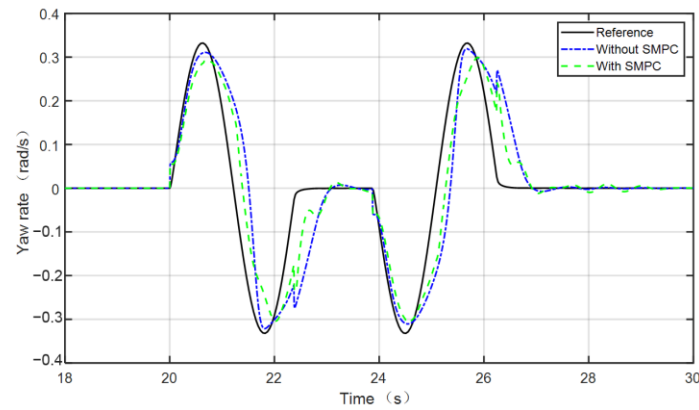


Figure 8. Comparison of yaw rate ($\mu = 0.8$).

As shown in Figure 9, when the road adhesion was set to 0.3 without an SMPC, the ASV lost control, and the error between its lateral distance and the desired routine kept increasing over the course of the double-lane change. With the control of an SMPC, the ASV maintained the vehicle trajectory error within a certain range.

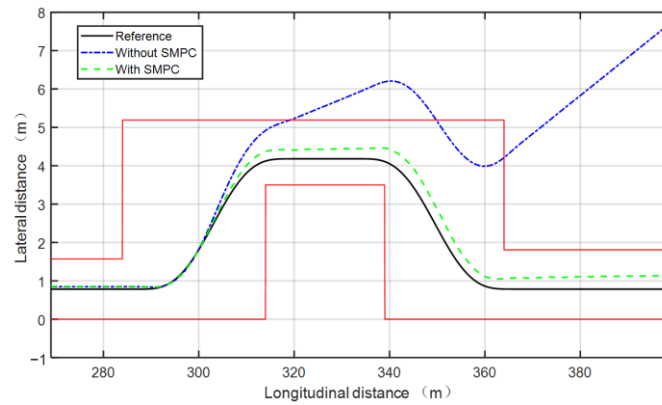


Figure 9. Comparison of vehicle trajectory ($\mu = 0.3$).

As shown in Figure 10, without an SMPC, the vehicle yaw rate was bigger than the yaw rate gained from the reference model. The gap in vehicle yaw rate between the vehicle with an SMPC was smaller than the gap without it.

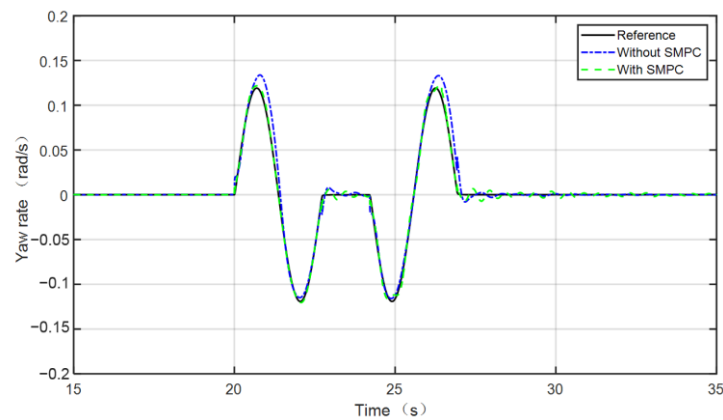


Figure 10. Comparison of yaw rate ($\mu = 0.3$).

The RMSE (Root Mean Square Error) and MAE (Maximum Absolute Error) of the vehicle trajectory and yaw rate during the double-lane change process were calculated and compared, as shown in Table 2.

Table 2. RMSE and MAE of the vehicle trajectory and yaw rate.

Road Adhesion	Indicator	RMSE		MAE	
		Without SMPC	With SMPC	Without SMPC	With SMPC
$\mu=0.8$	Trajectory	0.013	0.004	0.51	0.19
	Yaw rate	0.033	0.017	0.23	0.18
$\mu=0.3$	Trajectory	0.211	0.013	6.91	0.32
	Yaw rate	0.0013	0.0007	0.02	0.01

RMSE judges the global error in the whole range, while MAE indicates the maximum error of the peak value. For these two indicators, a lower value means better performance. In Table 1, both the RMSE and MAE decreased dramatically when the vehicle was equipped with an SMPC. Therefore, the designed SMPC can improve the path-tracking ability of ASV.

5. Conclusions

An ASV usually works in sealing or semi-sealing areas, where the working conditions are simpler than the passenger vehicle. Autonomous driving for an ASV can save on labor and decrease potential risks, which makes it meaningful and practical. The path-tracking ability is one of the fundamental functions of autonomous driving. A path-tracking model and the SMPC method were provided based on vehicle dynamic theory to improve an ASV's path-tracking performance. Its effectiveness was validated by double-lane change conditions on a road with different road adhesion coefficients. The simulation was conducted on the HIL platform. According to the simulation, with the provided SMPC controller, the path-tracking error decreased by 21.73~93.84%. The designed SMPC improved the vehicle path-tracking performance, thus laying a good foundation for autonomous driving for ASV.

However, for the provided strategy, the robustness against environmental noise and interference should be further analyzed and improved before it is field tested.

Author Contributions: Conceptualization, S.Z. and B.H.; methodology, S.Z. and L.M.; software, D.P.; validation, L.M.; writing—original draft preparation, S.Z.; visualization, D.P.; project administration, B.H. All authors have read and agreed to the published version of the manuscript.

Funding: This research was funded by the Innovative Research Team Development Program of the Ministry of Education of China (IRT_17R83), the 111 Project (B17034) of China.

Institutional Review Board Statement: Not applicable.

Informed Consent Statement: Not applicable.

Data Availability Statement: The data used to support the findings of this study are available from the corresponding author upon request.

Conflicts of Interest: Author Shengzhi Zhong was employed by Liuzhou Wuling New Energy Automobile Co., Ltd. Author Dengzhi Peng was employed by the Dongfeng Off-Road Vehicle Co., Ltd. The remaining authors declare that the research was conducted in the absence of any commercial or financial relationships that could be construed as a potential conflict of interest.

References

- Wang, H.; Li, G.; Hou, J.; Chen, L.; Hu, N. A path planning method for underground intelligent vehicles based on an improved RRT* algorithm. *Electronics* **2022**, *11*, 294. [[CrossRef](#)]
- Yao, Q.; Tian, Y.; Wang, Q.; Wang, S. Control strategies on path tracking for autonomous vehicle: State of the art and future challenges. *IEEE Access* **2020**, *8*, 161211–161222. [[CrossRef](#)]
- Parekh, D.; Poddar, N.; Rajpurkar, A.; Chahal, M.; Kumar, N.; Joshi, G.P.; Cho, W. A review on autonomous vehicles: Progress, methods and challenges. *Electronics* **2022**, *11*, 2162. [[CrossRef](#)]
- Chen, T.; Chen, L.; Xu, X.; Cai, Y.; Sun, X. Simultaneous path following and lateral stability control of 4WD-4WS autonomous electric vehicles with actuator saturation. *Adv. Eng. Softw.* **2019**, *128*, 46–54. [[CrossRef](#)]

5. Zhang, L.; Wu, G. *Combination of Front Steering and Differential Braking Control for the Path Tracking of Autonomous Vehicle*; SAE Technical Paper No. 2016-01-1627; SAE International: Warrendale, PA, USA, 2016.
6. Yu, J.; Guo, X.; Pei, X.; Chen, Z.; Zhu, M.; Gong, B. *Robust Model Predictive Control for Path Tracking of Autonomous Vehicle*; SAE Technical Paper No. 2019-01-0693; SAE International: Detroit, MI, USA, 2019.
7. Hang, P.; Chen, X. Path tracking control of 4-wheel-steering autonomous ground vehicles based on linear parameter-varying system with experimental verification. *Proc. Inst. Mech. Eng. Part I J. Syst. Control Eng.* **2021**, *235*, 411–423. [[CrossRef](#)]
8. Peng, D.; Fang, K.; Kuang, J.; Hassan, M.A.; Tan, G. Conflict and sensitivity analysis of articulated vehicle lateral stability based on single-track model. *Shock. Vib.* **2021**, *2021*, 5893993. [[CrossRef](#)]
9. Dudziński, P.A. Problems of turning process in articulated terrain vehicles. *J. Terramech.* **1983**, *19*, 243–256. [[CrossRef](#)]
10. Yang, M.; Bian, Y.; Liu, G.; Zhang, H. Path tracking control of an articulated road roller with sideslip compensation. *IEEE Access* **2020**, *8*, 127981–127992. [[CrossRef](#)]
11. Shutnan, W.A.; Abdalla, T.Y. Artificial immune system based optimal fractional order PID control scheme for path tracking of robot manipulator. In Proceedings of the 2018 International Conference on Advance of Sustainable Engineering and its Application (ICASEA), Wasit, Iraq, 14–15 March 2018; pp. 19–24.
12. Xueyun, L.; Shuang, L.; Ju, Z. Robust controller design for trajectory tracking of autonomous vehicle. *Int. J. Veh. Perform.* **2020**, *6*, 381–398. [[CrossRef](#)]
13. Lee, K.; Im, D.Y.; Kwak, B.; Ryou, Y.J. Design of fuzzy-PID controller for path tracking of mobile robot with differential drive. *Int. J. Fuzzy Log. Intell. Syst.* **2018**, *18*, 220–228.
14. Peng, D.; Huang, B.; Huang, H. Design of an Anti-Windup PID Algorithm for Differential Torque Steering Systems. *Shock. Vib.* **2022**, *2022*, 9973379. [[CrossRef](#)]
15. Chen, H. Terminal sliding mode tracking controller design for Automatic Guided Vehicle. *IOP Conf. Ser. Mater. Sci. Eng.* **2018**, *322*, 072035. [[CrossRef](#)]
16. Ding, C.; Ding, S.; Wei, X.; Mei, K. Output feedback sliding mode control for path-tracking of autonomous agricultural vehicles. *Nonlinear Dyn.* **2022**, *110*, 2429–2445. [[CrossRef](#)]
17. Lakhekar, G.V.; Waghmare, L.M. Robust self-organising fuzzy sliding mode-based path-following control for autonomous underwater vehicles. *J. Mar. Eng. Technol.* **2023**, *22*, 131–152. [[CrossRef](#)]
18. Chen, C.; Li, M.; Sui, J.; Wei, K.; Pei, Q. A genetic algorithm-optimized fuzzy logic controller to avoid rear-end collisions. *J. Adv. Transp.* **2016**, *50*, 1735–1753. [[CrossRef](#)]
19. Banjanovic-Mehmedovic, L.; Baluković, A. PSO optimized fuzzy controller for mobile robot path tracking. In *New Technologies, Development and Application III 6*; Springer International Publishing: Cham, Switzerland, 2020; pp. 413–421.
20. Rokonzaman, M.; Mohajer, N.; Nahavandi, S.; Mohamed, S. Review and performance evaluation of path tracking controllers of autonomous vehicles. *IET Intell. Transp. Syst.* **2021**, *15*, 646–670. [[CrossRef](#)]
21. Li, H.; Huang, J.; Yang, Z.; Hu, Z.; Yang, D.; Zhong, Z. Adaptive robust path tracking control for autonomous vehicles with measurement noise. *Int. J. Robust Nonlinear Control.* **2022**, *32*, 7319–7335. [[CrossRef](#)]
22. Gu, J.; Fang, D. Genetic Algorithm Based LQR Control for AGV Path Tracking Problem. *J. Phys. Conf. Ser.* **2021**, *1952*, 032012. [[CrossRef](#)]
23. Wu, T. Path tracking control for a robot-trailer system with parameter tuning using particle swarm optimization. In Proceedings of the 2018 IEEE International Conference on Mechatronics and Automation (ICMA), Changchun, China, 5–8 August 2018; pp. 1257–1262.
24. Sun, N.; Zhang, W.; Yang, J. Integrated Path Tracking Controller of Underground Articulated Vehicle Based on Nonlinear Model Predictive Control. *Appl. Sci.* **2023**, *13*, 5340. [[CrossRef](#)]
25. Ren, M.; Wu, G.; Chen, X.; Liu, X. *Model Predictive Automatic Lane Change Control for Intelligent Vehicles*; SAE Technical Paper No. 2020-01-5025; SAE International: Warrendale, PA, USA, 2020.
26. Bai, G.; Liu, L.; Meng, Y.; Luo, W.; Gu, Q.; Ma, B. Path tracking of mining vehicles based on nonlinear model predictive control. *Appl. Sci.* **2019**, *9*, 1372. [[CrossRef](#)]
27. Huang, B.; Yuan, Z.; Peng, D.; Wei, X.; Wang, Y. Coordination Control of Active Steering and Direct Yaw Control for the Articulated Steering Vehicle. *Shock. Vib.* **2023**, *2023*, 5577119. [[CrossRef](#)]
28. Wang, N.; Gao, Y.; Zhang, X. Data-driven performance-prescribed reinforcement learning control of an unmanned surface vehicle. *IEEE Trans. Neural Netw. Learn. Syst.* **2021**, *32*, 5456–5467. [[CrossRef](#)] [[PubMed](#)]
29. Ma, H.; Chen, J.; Eben, S.; Lin, Z.; Guan, Y.; Ren, Y.; Zheng, S. Model-based constrained reinforcement learning using generalized control barrier function. In Proceedings of the 2021 IEEE/RSJ International Conference on Intelligent Robots and Systems (IROS), Prague, Czech Republic, 27 September–1 October 2021; pp. 4552–4559.
30. Khandekar, A.A.; Malwatkar, G.M.; Kumbhar, S.A.; Patre, B.M. Continuous and discrete sliding mode control for systems with parametric uncertainty using delay-ahead prediction. In Proceedings of the 2012 12th International Workshop on Variable Structure Systems, Mumbai, Maharashtra, India, 12–14 January 2012; pp. 202–207.

Disclaimer/Publisher’s Note: The statements, opinions and data contained in all publications are solely those of the individual author(s) and contributor(s) and not of MDPI and/or the editor(s). MDPI and/or the editor(s) disclaim responsibility for any injury to people or property resulting from any ideas, methods, instructions or products referred to in the content.